

Conventional and diffusion-weighted MRI of extrahepatic hydatid cysts

Nagihan Inan, Nilay Akhun, Gür Akansel, Arzu Arslan, Ercüment Çiftçi, Ali Demirci

PURPOSE

To evaluate the value of conventional and diffusion-weighted (DW) magnetic resonance imaging (MRI) in the diagnosis of extrahepatic hydatid cysts.

MATERIALS AND METHODS

Forty-one extrahepatic hydatid cysts (12 renal, 6 pulmonary, 5 peritoneal, 4 bone, 3 soft tissue, 3 pancreatic, 2 splenic, 2 retroperitoneal, 1 adrenal, 1 scrotal, 1 diaphragmatic, and 1 cardiac) were included in this retrospective study. After a series of routine conventional MRI, DW imaging was performed using a breath-hold, single-shot, echo-planar, spin echo sequence with three b factors (0, 500 and 1,000 s/mm²), and apparent diffusion coefficient (ADC) maps were created. On DW trace images, signal intensity of the cysts was visually compared to the signal intensity of the muscle with the use of a 3-point scale: 0, isointense; 1, moderately hyperintense; 2, significantly hyperintense. For quantitative evaluation, signal intensity ratio and ADC of the cystic lesions were calculated.

RESULTS

On conventional MR images, all but 3 patients had concomitant liver involvement. Three of them were disseminated. On DW trace images (b = 1,000 s/mm²), most hydatid cysts (86%) were hyperintense, while five hydatid cysts (14%) were isointense. Quantitatively, the mean ADC of the hydatid cysts was $2.8 \times 10^{-3} \pm 0.5 \text{ mm}^2/\text{s}$.

CONCLUSION

DW imaging may help in the differential diagnosis of extrahepatic hydatid cysts.

Key words: • hydatid cyst • diffusion weighted imaging • magnetic resonance imaging

Although liver (75%) and lung (15%) are the most commonly involved organs with hydatid disease, hydatid cysts (HCs) can affect almost anywhere in the body (1). The diagnosis of these cysts is usually made by some characteristic radiologic features and positive serology. Radiologic appearance of HCs depends on the stage of maturity and ranges from completely liquid type to completely solid type (2). The diagnostic accuracy is high for cysts with characteristic features such as a visible cyst wall (seen as a low signal intensity rim on T2-weighted magnetic resonance images), multivesicular appearance, floating membrane, and calcification (3). However, unusual sites and appearances may cause diagnostic difficulties (1, 4). In addition, initial phase HCs usually appear as a well-defined unilocular anechoic cyst (completely liquid type), and are therefore radiologically indistinguishable from simple cysts (2).

In this study, we evaluated the contribution of diffusion-weighted imaging (DWI) in the diagnosis of extrahepatic HCs, which pose a challenge in the diagnosis both on US and conventional magnetic resonance imaging (MRI).

Materials and methods

Patients

Our retrospective data were obtained through a 2-year period (September 2006 to September 2008). During this period 22 patients were referred for MRI for the following indications: suspected HC based on findings of other imaging modalities and evaluation for extrahepatic involvement in patients with known primary liver hydatid disease. However, 12 cysts in 7 patients were excluded from the study because of size (n=1), partial or complete calcification (n=6), low image quality of DW images (n = 2), and incomplete characterization of lesions on follow-up imaging or histopathologic examination (n=3). As a consequence, a total of 41 non-calcified extrahepatic hydatid cysts in 15 patients (5 women, 10 men) with a diameter of at least 1 cm were included in this study. Of the cysts, 2 were splenic, 3 were pancreatic, 12 were renal, 1 was adrenal, 5 were peritoneal, 2 were retroperitoneal, 6 were pulmonary, 1 was scrotal, 4 were osseous, 3 were soft tissue, 1 was diaphragmatic, and 1 was cardiac. Eight patients had multiple cysts. The distribution of cysts within specific organs, stage of cysts, and combination of simultaneous multi-organ involvement are presented in Table 1.

Imaging was performed prior to treatment or biopsy. The diagnosis of HCs was confirmed by biopsy in 9 patients (the presence of scolices or hooklets in the hydatid liquid), and/or positive serology for hydatidosis in 15 patients (hemagglutinin inhibition [HAI] positive for dilutions 1/160). For subjects with multiple HCs only one lesion

From the Department of Radiology (N.I. ✉ nagihaninan@yahoo.com.tr), Kocaeli University School of Medicine, Kocaeli, Turkey.

Received 7 June 2009; revision requested 23 July 2009; revision received 24 July 2009; accepted 29 July 2009.

Published online 4 February 2010
DOI 10.4261/1305-3825.DIR.2892-09.1

Table 1. Distribution of hydatid cysts within specific organs, stage of cysts, and combinations of simultaneous multi-organ involvement

Patient	Hepatic involvement	Extrahepatic sites of involvement	Stages of hydatid cysts (n)
1	+	soft tissue	stage 2 (1)
2	+	renal	stage 1 (2)
3	+	bone	stage 1 (1)
4	+	adrenal gland	stage 1 (1)
5	+	soft tissue bone scrotum	stage 1 (2) stage 2 (2) stage 2 (1)
6	+	renal diafragmatic pancreatic peritoneal retroperitoneal pulmonary	stage 1 (1) stage 1 (1) stage 1 (2) stage 2 (4) stage 3 (1) stage 2 (1)
7	+	renal pancreatic peritoneal pulmonary splenic	stage 3 (1) stage 1 (1) stage 1 (1) stage 1(1) stage 3 (1)
8	+	pulmonary	stage 1 (2)
9	-	bone pulmonary	stage 2 (1) stage 1 (1)
10	+	pulmonary	stage 3 (1)
11	-	renal	stage 1 (1)
12	-	renal splenic	stage 1 (3) stage 1 (1)
13	+	renal	stage 1 (4)
14	+	retroperitoneal	stage 2 (1)
15	+	cardiac	stage 1 (1)

was analyzed histopathologically. The remainder of lesions with similar or characteristic radiologic appearance was accepted as HCs.

The study was approved by the institutional review board and protocol review committee.

Magnetic resonance imaging

All patients were examined with a 1.5 Tesla MR scanner (Gyrosan Intera; Philips Medical Systems, Best, The Netherlands) using a four element phased-array body coil. This system has a maximal gradient strength of 30 mT/m and a slew rate of 150 mT/m/ms. All patients were examined initially with our routine MRI protocol that included for the abdomen and mediastinum precontrast axial T1-

weighted, breath-hold, spoiled gradient echo (fast field echo, FFE), with and without fat suppression (TR/TE/FA/NEX, 169/4.6/80/1), coronal and axial T2-weighted, single shot, turbo spin echo (SS-TSE) (TR/TE/NEX/TSE factor, 700/80/1/72), and axial T2-weighted SS-TSE with fat suppression (TR/TE/NEX/TSE factor, 700/80/1/72); for the soft tissue and bone precontrast, axial, T1-weighted, TSE, with and without fat suppression (TR/TE/TSE factor/NEX, 500/18/5/2), coronal and axial T2-weighted TSE (TR/TE/NEX/TSE factor, 2000/100/5/2), and axial T2-weighted TSE with fat suppression. Subsequently, 3 series of axial, single-shot, spin-echo, echo-planar (SS-SE-EP) DW images (TR/TE/echo-planar imaging factor, 1000/81/77;

sensitizing gradients in x, y, z directions) were acquired using b values of 0, 500 and 1,000 s/mm². ADC maps were reconstructed from these images. Fat suppression was performed by using spectral saturation inversion recovery (SPIR) technique. DWI consisted of a multisection acquisition with a slice thickness of 6 mm, an intersection gap of 1 mm, and an acquisition matrix of 128 × 256. All sequences were acquired using a partially-parallel imaging acquisition and SENSE reconstruction with a reduction factor (R) of 2. For abdominal imaging, the acquisition period of each DWI series during a single breath-hold was 26 seconds.

Analysis of MR images

For qualitative analysis on conventional MR images, cyst size, sites of involvement, and imaging findings were evaluated. All HCs were classified according to the World Health Organization classification (3). Completely liquid type refers to unilocular cystic lesions with uniform anechoic contents, without a visible wall (type CL); type 1 refers to a univesicular cyst with a visible cyst wall (type CE1); type 2 refers to a multivesicular cyst (type CE2); type 3 refers to a cyst with a floating membrane (type CE3). Types CE4 and CE5 (completely or partially calcified cysts) were not included in our study.

On DW images with b factor of 1000 s/mm², signal intensity (SI) of the cysts relative to the muscle was visually assessed with the use of a 3-point scale as follows: 0, isointense; 1, moderately hyperintense; 2, significantly hyperintense. All images were independently assessed by two radiologists (NI, NA) who were blinded to the clinical history and results of the prior imaging studies. Results of the interpretations were then compared. In four cases, for which the results differed, the final score was reached with consensus achieved after discussion.

For quantitative analysis, images were transferred to a dedicated workstation (Dell Workstation Precision 650, View Forum release 3.4). SI of the cysts and affected tissue were measured by one of the radiologists (NI) for each b factor (0, 500 and 1,000 s/mm²) using a region of interest (ROI) of the same size. The ROI

was placed centrally and the size of the ROI was kept as large as possible, covering at least two-thirds of the cyst, yet avoiding interference from the surrounding tissue and major blood vessels. In addition, the ADC maps were created automatically and the mean ADC values of cysts were determined on images with b factors of 0 and 1,000 s/mm². The average of three measurements was recorded as the final SI or ADC. Cyst-to-affected tissue SI ratio (SIR), and ADC of HCs were calculated.

Results

Qualitative analysis

The mean age of patients was 44.5 years (range, 15–67 years). The cyst diameter range was 16–181 mm. The distribution of cysts within specific organs, stage of cysts, and combinations of simultaneous multi-organ involvement are listed in Table 1. Eleven renal, 1 adrenal, 2 soft tissue, 1 osseous, 1 diaphragmatic, 3 pancreatic, 1 peritoneal, 4 pulmonary, and 1 splenic HC had univesicular appearance without any internal structure (type 1); 1 soft tissue, 3 osseous, 1 pulmonary, 1 scrotal, 4 peritoneal, and 1 retroperitoneal cyst had multivesicular appearance (type 2); 1 renal, 1 pulmonary, and 1 retroperitoneal cyst had a floating membrane (type 3). Except for 3 patients (one had isolated renal involvement, another had concomitant renal and splenic involvement, yet another had concomitant lung and bone involvement), all patients (n = 11) had concomitant liver involvement. Three of them had disseminated involvement (one of them had concomitant scrotal, osseous, and soft tissue involvement; another had concomitant pulmonary, pancreatic, diaphragmatic, peritoneal, and retroperitoneal involvement; yet another had pulmonary, renal, splenic, peritoneal, and retroperitoneal involvement).

Results of the visual evaluation of the SI on DW images with a b factor of 1,000 s/mm² are shown in Table 2. With the exception of 6, most HCs were moderately or significantly hyperintense on DW images with a b factor of 1,000 s/mm² (Figs. 1–3).

Quantitative analysis

The results of quantitative analysis of DWI are outlined in Table 3.

Table 2. Visual evaluation of MR signal intensities of hydatid cysts on diffusion trace images (b = 1000 s/mm²)

MR signal intensity	Hydatid cysts (n = 41)
Significantly hyperintense	8 (20%)
Moderately hyperintense	27 (66%)
Isointense	6 (14%)

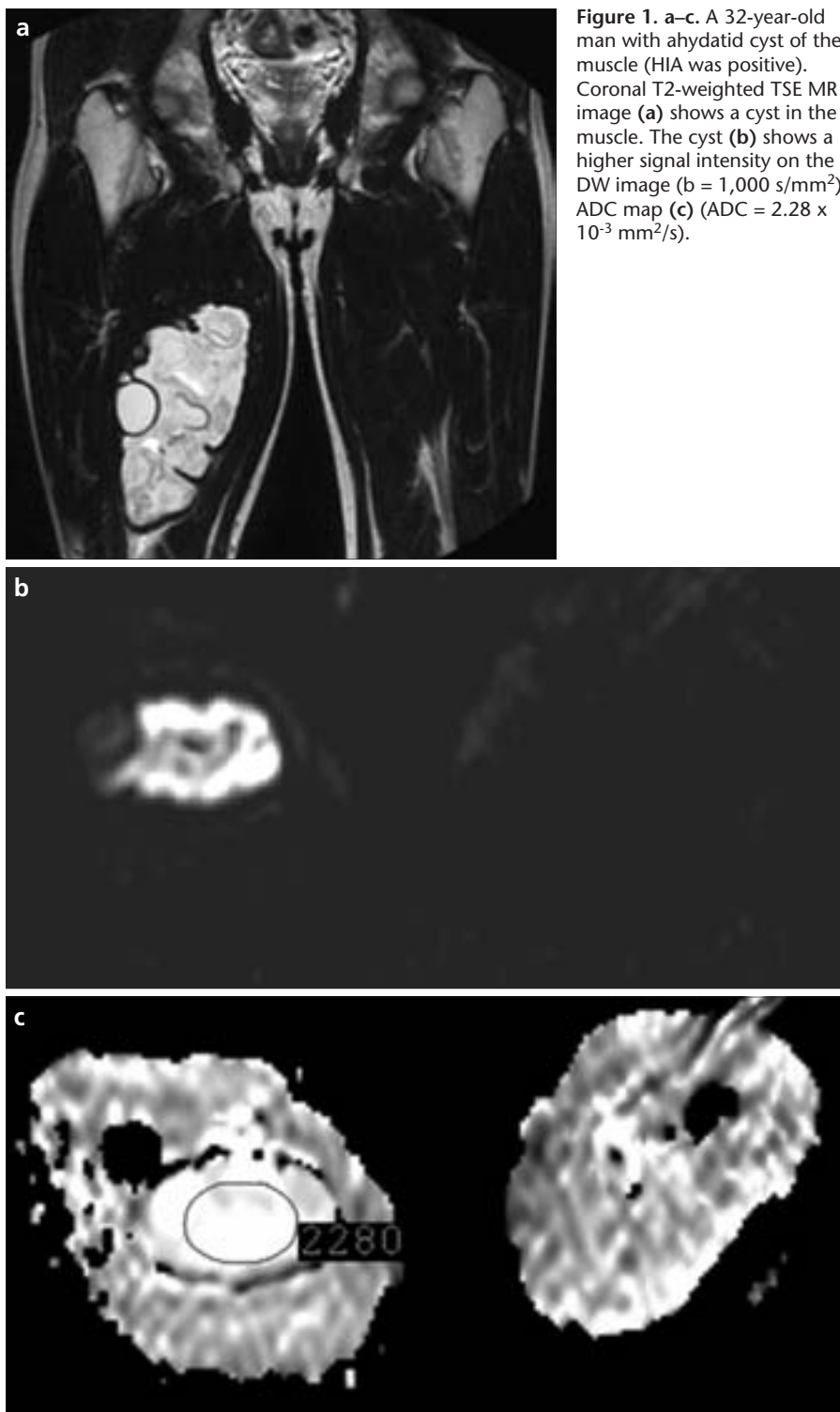


Figure 1. a–c. A 32-year-old man with a hydatid cyst of the muscle (HIA was positive). Coronal T2-weighted TSE MR image (a) shows a cyst in the muscle. The cyst (b) shows a higher signal intensity on the DW image (b = 1,000 s/mm²). ADC map (c) (ADC = 2.28 × 10⁻³ mm²/s).

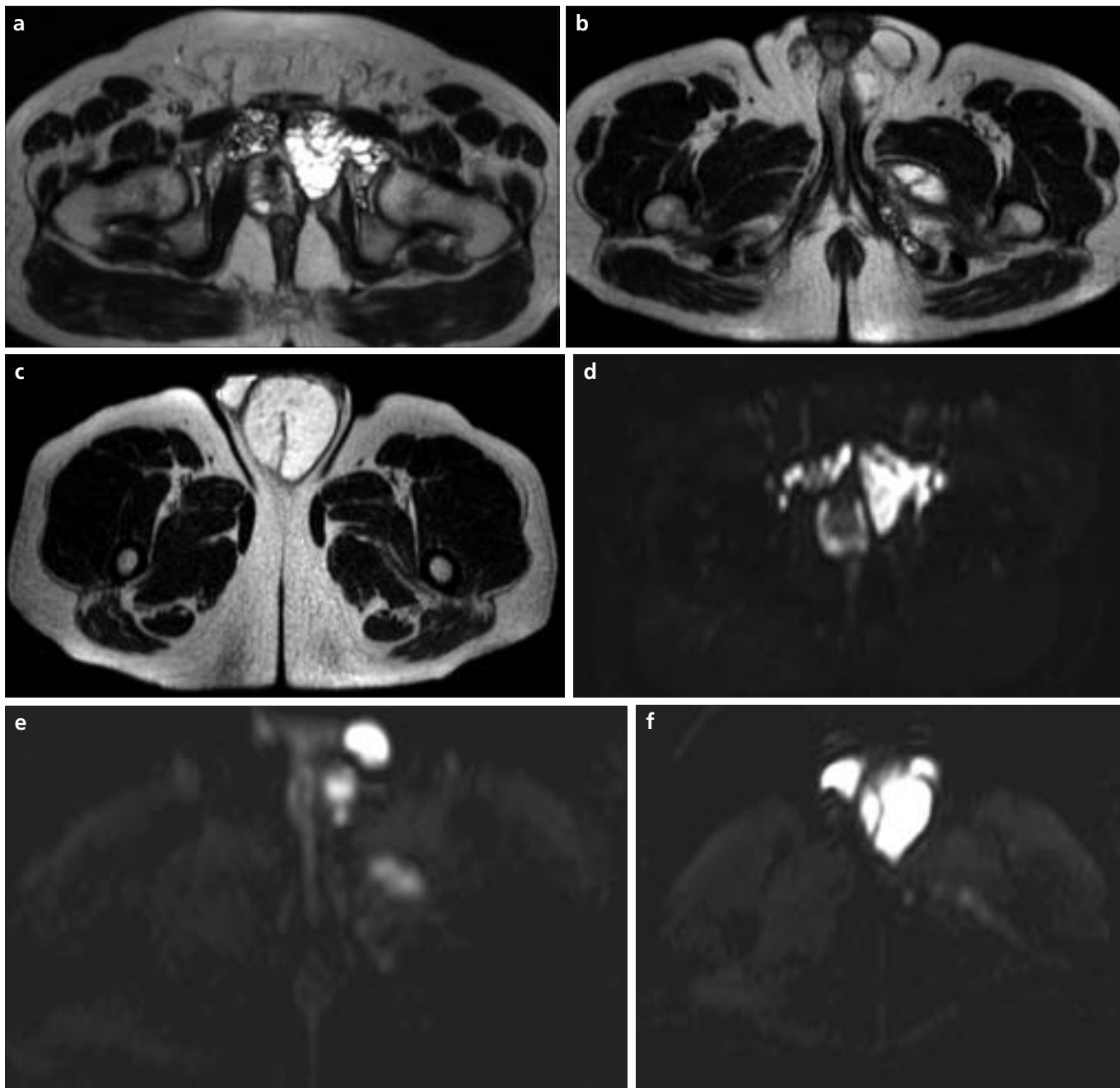


Figure 2. a–i (continued on next page). A 49-year-old man with hydatid cysts of the bone, scrotum, and muscle (HIA was positive). Axial T2-weighted TSE MR images (a–c) show cysts in the bilateral pubic rami, scrotum, and muscle. The cysts (d–f) show a higher signal intensity on DW images ($b = 1,000 \text{ s/mm}^2$).

Table 3. Quantitative analysis of DWI of hydatid cysts ($b = 500$ and $1,000 \text{ s/mm}^2$)

	Hydatid cysts ($n = 41$)
SIR ($b = 1000 \text{ s/mm}^2$)	2.2 ± 2.2
ADC ($\times 10^{-3} \text{ mm}^2/\text{s}$)	2.8 ± 0.5

Data are mean \pm SD.
SIR, signal intensity ratio; ADC, apparent diffusion coefficients.

Discussion

On conventional MRI, the diagnostic accuracy is high for HCs with specific imaging features such as a hypointense wall on T2-weighted images, a floating membrane, and daughter cysts (5). However, imaging features of HCs may sometimes overlap with those of other cystic lesions. For example, both simple cysts and complete liquid type HCs display high SI on T2-

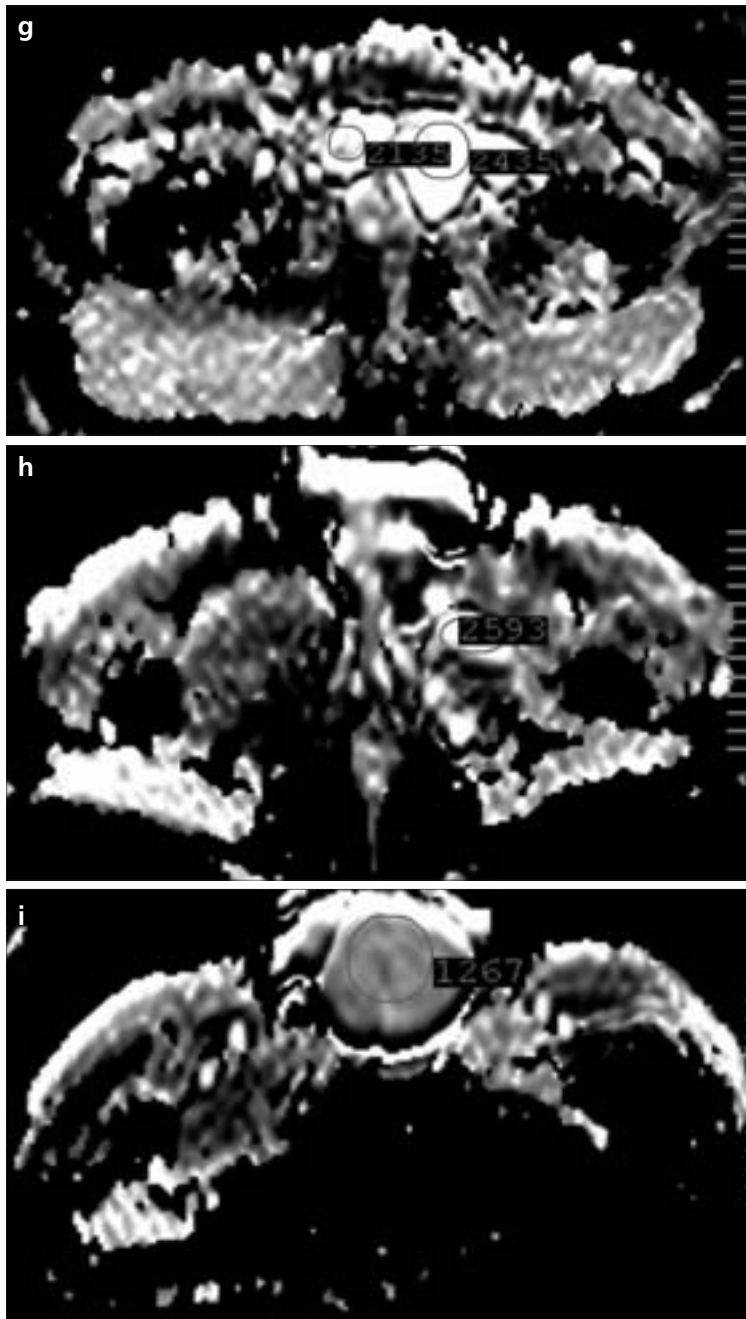


Figure 2. a-i (continued from previous page). ADC maps (g-i) (ADCs are 2.1×10^{-3} , 2.4×10^{-3} , 2.6×10^{-3} , and 1.3×10^{-3} mm^2/s for the right superior pubic ramus, left superior pubic ramus, muscle, and scrotum, respectively).

weighted and low SI on T1-weighted images, with well-defined margins. In these patients, careful evaluation of the patient's clinical history and laboratory findings are important for differential diagnosis. In contrast to a simple cyst, HCs usually have a wall which shows low signal intensity on T2-weighted images (rim sign) (1, 4). However, this finding is not specific because it can also be seen with some

other cystic lesions such as abscesses, necrotic tumors, and hematomas.

Recent reports have suggested that DWI can be helpful in the characterization of cystic lesions in the abdomen or brain, such as simple cysts, HCs, and liver abscesses, ovarian and endometrial cystic neoplasms, arachnoid and epidermoid cysts, with high specificity and sensitivity (6–10). In these studies, the difference in ADCs

of cysts was attributed to the difference in cellular density. To our knowledge, except for hepatic HCs, the role of DWI in the differential diagnosis of extrahepatic cysts has not been reported previously.

In our study, most of the HCs were hyperintense on images with a b factor of $1,000 \text{ s}/\text{mm}^2$ in which the contribution of the T2 “shine-through” to the SI decreases while tissue cellularity makes a greater contribution (11). In addition, diffusion can be quantitatively evaluated by ADC, which is free of the T2 shine-through effect (12). In our series, the mean ADC of the HCs was 2.8 ± 0.5 . However, we did not compare ADCs of these cysts with simple cysts, because there were not simple cysts in all affected tissues covered in our study. However, our previous studies (which were done with the same 1.5 Tesla MRI scanner and parameters) showed that DWI with SS EPI may be helpful in the characterization of hepatic (7) and pancreatic (12) cysts, with high specificity and sensitivity. In these studies, the ADC of the hepatic HCs were significantly lower than those of hepatic simple cysts (mean ADCs were $3.5 \times 10^{-3} \text{ mm}^2/\text{s} \pm 0.5$ and 2.2 ± 0.8 for simple cysts and HCs, respectively) and the ADC of pancreatic HCs were significantly lower than those of pancreatic simple cysts (mean ADCs were $3.3 \times 10^{-3} \text{ mm}^2/\text{s} \pm 0.5$ and $2.6 \times 10^{-3} \text{ mm}^2/\text{s} \pm 0.2$ for simple cysts and HCs, respectively). When the results from this study are compared with those from our previous studies, it appears that the ADC values of HCs in the current study are lower than those of simple cysts. Therefore, the high signal on DW images and the low ADCs are probably due to the reduced diffusion in HCs which can be attributed to the differences in the cyst contents. Since the HCs have a viscous content which consists of scolices, hooklets, sodium chloride, proteins, glucose, ions, lipids, and polysaccharides, they have a decreased ADC (13, 14). On the contrary, simple cysts contain serous fluid, thus a higher ADC.

This study has several technical limitations. The main limitation is that the EPI sequence employed with a higher b value had a lower SNR, resulting in greater image distortion. In addition, EPI sequence causes anatomic distortion due to susceptibility effects (11).

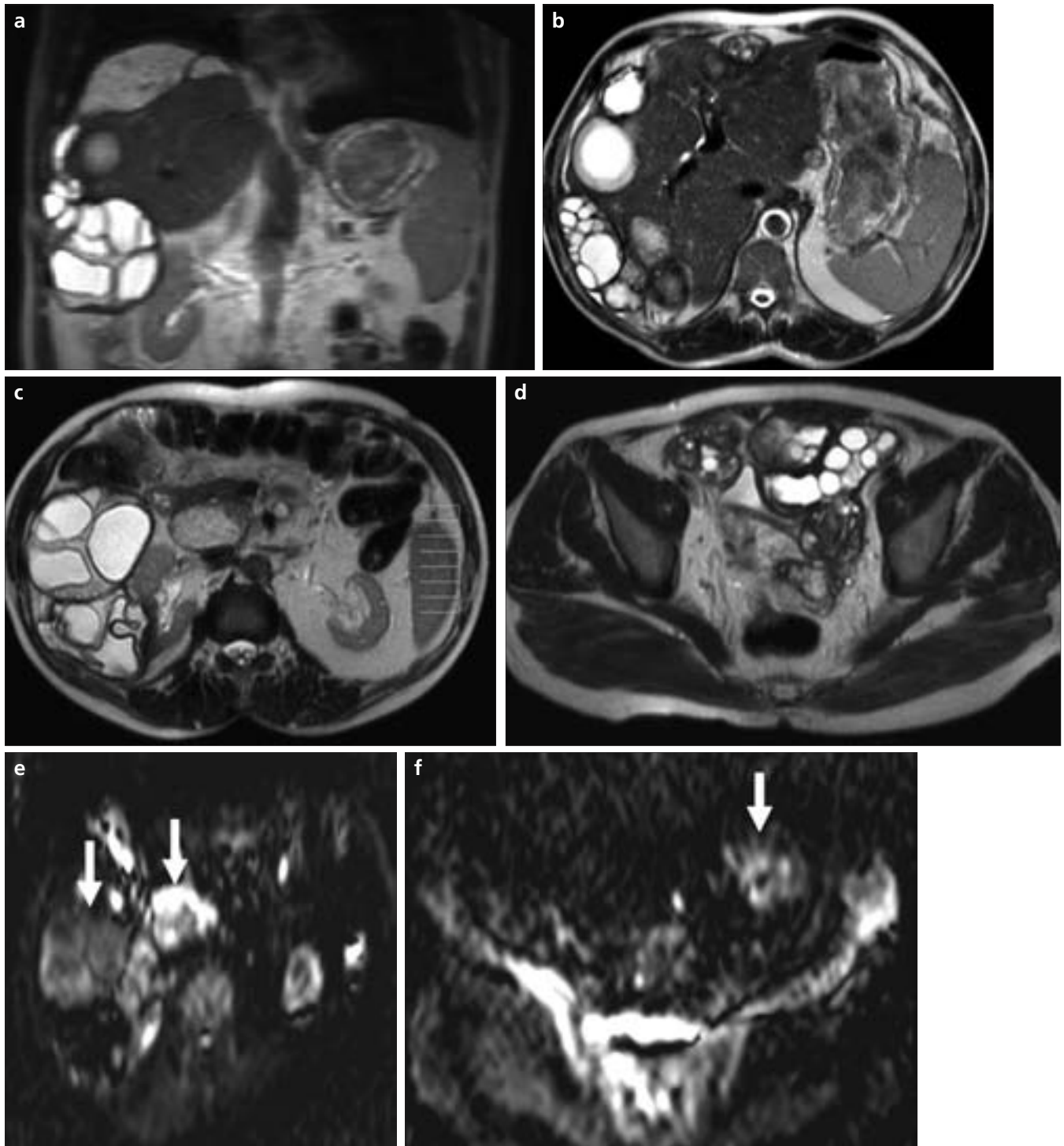


Figure 3. a–f. A 63-year-old man with disseminated hydatid disease (HIA was positive). Coronal (a) and axial (b–d) T2-weighted TSE MR images show cysts in the pancreas, diaphragm, intraperitoneal, and retroperitoneal areas. The cysts (arrows, e, f) show higher signal intensity than the liver on DW images ($b = 1,000 \text{ sec/mm}^2$). On ADC maps ADCs were 2.5×10^{-3} ; 2.1×10^{-3} ; and $2.3 \times 10^{-3} \text{ mm}^2/\text{s}$, respectively.

Another important limitation is the lack of simple cysts in similar localizations for comparison. Further studies on larger series comparing hepatic with simple cysts are needed.

The differential diagnosis of HCs is usually possible with the combined

use of specific morphologic features on imaging, laboratory, and clinical information. However, sometimes the differential diagnosis of the HCs from simple cysts may still be difficult. Especially in endemic areas, the radiologist must be careful because some-

times HCs may simulate a malignant cystic tumor or a benign simple cyst on MRI. Our preliminary data suggest that DWI may be helpful in this setting and this sequence can be easily added to the routine protocol because of short examination time.

References

1. Ilica AT, Kocaoglu M, Zeybek N, et al. Extrahepatic abdominal hydatid disease caused by *Echinococcus granulosus*: imaging findings. *AJR Am J Roentgenol* 2007; 189:337–343.
2. Caremani M, Lapini L, Caremani D, Occhini U. Sonographic diagnosis of hydatidosis: the sign of the cyst wall. *Eur J Ultrasound* 2003; 16:217–223.
3. WHO Informal Working Group. International classification of ultrasound images in cystic echinococcosis for application in clinical and field epidemiological settings. *Acta Trop* 2003; 85:253–261.
4. Andronikou S, Welman CJ, Kader E. Classic and unusual appearances of hydatid disease in children. *Pediatr Radiol* 2002; 32:817–828.
5. Singh S, Gibikote SV. Magnetic resonance imaging signal characteristics in hydatid cysts. *Australas Radiol* 2001; 45:128–133.
6. Chan JH, Tsui EY, Luk SH, et al. Diffusion-weighted MR imaging of the liver: distinguishing hepatic abscess from cystic or necrotic tumor. *Abdom Imaging* 2001; 26:161–165.
7. Inan N, Arslan A, Akansel G, et al. Diffusion-weighted imaging in the differential diagnosis of simple and hydatid cysts of the liver. *AJR Am J Roentgenol* 2007; 189:1031–1036.
8. Nakayama T, Yoshimitsu K, Irie H, et al. Diffusion-weighted echo-planar MR imaging and ADC mapping in the differential diagnosis of ovarian cystic masses: usefulness of detecting keratinoid substances in mature cystic teratomas. *J Magn Reson Imaging* 2005; 22:271–278.
9. Hakyemez B, Aksoy U, Yildiz H, Ergin N. Intracranial epidermoid cysts: diffusion-weighted, FLAIR and conventional MR findings. *Eur J Radiol* 2005; 54:214–220.
10. Chen S, Ikawa F, Kurisu K, et al. Quantitative MR evaluation of intracranial epidermoid tumors by fast fluid-attenuated inversion recovery imaging and echo-planar diffusion-weighted imaging. *AJNR* 2001; 22:1089–1096.
11. Naganawa S, Kawai H, Fukatsu H, et al. Diffusion-weighted imaging of the liver: technical challenges and prospects for the future. *Magn Reson Med Sci* 2005; 4:175–186.
12. Inan N, Arslan A, Akansel G, Anik Y, Demirci A. Diffusion-weighted imaging in the differential diagnosis of cystic lesions of the pancreas. *AJR Am J Roentgenol* 2008; 191:1115–1121.
13. Volders WK, Gelin G, Stessens RC. Best cases from the AFIP. Hydatid cyst of the kidney: radiologic-pathologic correlation. *Radiographics* 2001; 21:255–260.
14. Pedrosa I, Saiz A, Arrazola J, Ferreiros J, Pedrosa CS. Hydatid disease: radiologic and pathologic features and complications. *Radiographics* 2000; 20:795–817.